S0168-9274(05)00062-0/FLA AID:1766 Vol.●●●(●●●)
APNUM:m2 v 1.36 Prn:25/03/2005; 8:35
anm1766
[DTD5] P.1 (1-29)
by:ML p. 1

Available online at www.sciencedirect.com

SCIENCE DIRECT®

Applied Numerical Mathematics ●●● (●●●●) ●●●–●●●

APPLIED NUMERICAL MATHEMATICS

www.elsevier.com/locate/apnum

Continuous metrics and mesh adaptation

Francois Courty [a], David Leservoisier [b], Paul-Louis George [c], Alain Dervieux [a,*]

[a] *INRIA, BP 93, 06902 Sophia Antipolis, France*
[b] *SNECMA – Villaroche, 77550 Moissy-Cramayel, France*
[c] *INRIA, BP 105, 78153 Le Chesnais, France*

Abstract

This paper addresses the problem of finding the mesh representing at best in L^p a twice continuous differentiable function defined on the plane. A continuous setting of this problem is used. It relies on an abstract mesh model, the "continuous metrics" allowing a variational analysis and on the identification of an optimum. Anisotropic optimal meshes can then be specified. An extension to discontinuities is proposed. It involves the prediction of the convergence order of the underlying mesh adaptation method. We present a few numerical illustrations related to numerical solution representation and to image compression.

Keywords: Mesh; Adaptation; Approximation; Interpolation; Compression; Metrics

1. Introduction

CFD researchers have spent decades constructing "second-order accurate schemes" but when they are applied to industrial problems, numerical convergence is rarely second order. When theorists are addressed about this problem, they answer that the Navier–Stokes flow fields are generally smooth but they involve steep gradients, and therefore it might happen that second-order convergence, only an asymptotical property, will indeed apply, but only for extremely fine meshes that are not usable in practice. Further, some of the flows of interest involve genuine singularities and second-order convergence cannot be obtained.

* Corresponding author.
E-mail address: alain.dervieux@inria.fr (A. Dervieux).

0168-9274/$30.00 © 2005 Published by Elsevier B.V. on behalf of IMACS.
doi:10.1016/j.apnum.2005.03.001

In fact, in order to answer to the expectation of these practitioners, a new theory of approximation, taking into account mesh adaptation is being progressively built by the research community. Indeed, uniform mesh refinement is identified as a penalizing option for higher-order mesh convergence.

With mesh adaptive approaches, the numerical order of the convergence to the continuous is routinely evaluated from the variation of error with respect to the number of nodes and appears as much better than with uniform mesh refinement (see, for example, [21]). This is due to advances in adaptation criteria and in mesh representation.

New theoretical developments are specifying progressively criteria for adapting meshes in order to get an error lower than a prescribed threshold. The derivation of *a posteriori* errors is an important topic in this direction, see, for example, [1,3,10].

However the relations between the adaptation strategy and the convergence order remain a difficult issue.

The adapted mesh needs not only to be fine enough in some regions, but also to be not too fine in other regions. It becomes a part of the unknowns in the system to solve. In the case where the mesh should be found among a set of deformations of a reference one, many works in the literature proposed the mesh deformation or equivalently mesh coordinates as the solution of a particular system coupled with the discrete partial differential equation (PDE) under study. See, for example, [6,17]. In that case the mesh topology is prescribed by the user and may be not adequate for the adaptation.

Conversely, in the case where the user does not wish to fix the topology, but instead, wants the algorithm to find it, then the definition of a system the solution of which is the adapted mesh is much more difficult. Firstly, two meshes can have very different topologies and give about the same local accuracy. Secondly, it is difficult to find an optimal mesh if we have to investigate inside a set of meshes described by integers and/or booleans.

These remarks have motivated researchers to represent meshes by continuous functions describing the mesh. See, for example, [2]. These functions can be for example the (scalar) local mesh density over the computational domain. From its knowledge, it is possible to derive an upper bound for the local truncation error. But this upper bound does not give a perfect idea of the local error if local stretching effects are not taken into account.

In many recent publications, see, for example, [4,5,12,13], the local stretching is modelled by means of a non-scalar field, the *metric*. An adapted metric is specified by an argument of equidistribution of an interpolation error related to the partial differential equation solution.

The main purpose of the present work is to explore several outputs of an analysis in which we look for the optimal metric in a *continuous setting*.

In the first step presented in this paper, we focus on the easier problem of adapting a mesh to the *best $\mathcal{P}_1$ interpolation of a given analytic function*. Interpolation errors have been the subject of many studies, in particular for mesh quality purposes (see, for example, [20,15]). From error estimates, abstract error models can be built. The problem of the best adapted metric can be cast into the optimization of this error model and the optimal metric can be exhibited. The mathematical model also allows to reproduce some convergence-to-the limit behaviors, giving some prediction of numerical convergence order for the discrete case.

We shall first consider the 1D case and recall how a continuous metric is defined, how the interpolation error can be modelled, and how a calculus of variation produces an optimal metric. The interpolation of a function having a discontinuity is analysed. The 1D case allows for an overview of several possible extensions.

S0168-9274(05)00062-0/FLA AID:1766 Vol.●●●(●●●) APNUM:m2 v 1.36 Prn:25/03/2005; 8:35 anm1766 [DTD5] P.3 (1-29) by:ML p. 3

Then we shall propose a model for the 2D case. The error model will be derived from an accurate error estimate. Then again we propose a definition of the best metric. This time, mesh anisotropy can be taken into account. The convergence order for isotropic and anisotropic adapted meshes is compared in the case of a discontinuous function.

We complete these theoretical statements by a series of numerical experiments in order to show examples for which behavior predicted by the theory are indeed observed. We finally illustrate how the "best interpolation" problem that we address can also applied to an image compression problem.

2. Continuous metric in an interval

This section is somewhat close to the end of Chapter 3 in [2] in which the authors look for the best mesh density. However we introduce in a different-purely continuous-setting the notion of metric optimality which will be the central tool of the sequel. After some definitions concerning the metric, we recall an estimate of the interpolation error and then show how an optimal metric can be derived.

2.1. Definitions

A metric on a given set allows to define the distance between two arbitrary elements of it. We shall call the metric on the interval $[a,b]$ a (strictly) positive continuous function $\mathcal{M}: x \to \mathcal{M}(x)$ defined on $[a,b]$. It specifies, for any c and d of this interval the length of segment cd as follows:

$$L_{\mathcal{M}}(cd) = \int_c^d \sqrt{\mathcal{M}}(s)\,\mathrm{d}s. \tag{1}$$

Let us consider a mesh of interval $[a,b]$ with N nodes. It is a subdivision $x_0 = a < x_1, \ldots, x_i < x_{i+1}, \ldots, x_{N-1} < x_N = b$ of this interval. A consequence of the above definition is that a metric can prescribe a particular class of meshes. Indeed, we shall say that a mesh conforms to metric $\mathcal{M}$ if and only if the following relation, unitary element length holds: *for any element* $[x_i, x_{i+1}]$, *we have* $\int_{x_i}^{x_{i+1}} \sqrt{\mathcal{M}}\,\mathrm{d}x = 1$.

In that case, if we introduce the local continuous mesh size $m_{\mathcal{M}} = \mathcal{M}^{-1/2}$ we have: *for any element* $[x_i, x_{i+1}]$, $\int_{x_i}^{x_{i+1}} \frac{1}{m_{\mathcal{M}}}\,\mathrm{d}x = 1$, which shows that when $m_{\mathcal{M}}$ is a constant function, it is nothing other than the element size.

Another way to view this is to introduce the local continuous node density $d_{\mathcal{M}} = 1/m_{\mathcal{M}}$: *for any interval* $[x_i, x_{i+1}]$, *we have* $\int_{x_i}^{x_{i+1}} d_{\mathcal{M}}(x)\,\mathrm{d}x = 1$.

It can be verified that the number of nodes (or equivalently intervals) of the mesh is specified by the metric. It is given by:

$$C(\mathcal{M}) = \int_a^b \sqrt{\mathcal{M}}\,\mathrm{d}x = \int_a^b 1/m_{\mathcal{M}}(x)\,\mathrm{d}x = \int_a^b d_{\mathcal{M}}(x)\,\mathrm{d}x. \tag{2}$$

If $C(\mathcal{M})$ is a positive integer, exactly one mesh is described by it, if $C(\mathcal{M})$ is not an integer, no mesh is described by it.

ARTICLE IN PRESS
S0168-9274(05)00062-0/FLA AID:1766 Vol.●●●(●●●) anm1766 [DTD5] P.4 (1-29)
APNUM:m2 v 1.36 Prn:25/03/2005; 8:35 by:ML p. 4

2.2. Interpolation error bound

The present work concentrates on the continuous $\mathcal{P}_1$ interpolation. We first recall in short an error bound useful for the sequel. We consider:

- A function u, regular enough, defined on a segment $[a,b]$,
- $h = \text{meas}([a,b])$, not necessarily small,
- $\Pi_h u$ the $\mathcal{P}_1$ interpolation of u on $[a,b]$: $\Pi_h u$ is an affine function on $[a,b]$, $(\Pi_h u)(a) = u(a)$, $(\Pi_h u)(b) = u(b)$,
- the approximation error defined by $e(x) = u(x) - (\Pi_h u)(x)$.

For any x in $[a,b]$, there exists t_1 and t_2 in $[0,1]$ such that:

$$e(a) = (u - \Pi_h u)(a) = (u - \Pi_h u)(x) + (a-x)(u - \Pi_h u)'(x) + \frac{(a-x)^2}{2} u''\big(x + t_1(a-x)\big),$$
$$e(b) = (u - \Pi_h u)(b) = (u - \Pi_h u)(x) + (b-x)(u - \Pi_h u)'(x) + \frac{(b-x)^2}{2} u''\big(x + t_2(b-x)\big).$$

Looking for an upper bound of $e = (u - \Pi_h u)$ leads to look for a point x such that $e'(x) = (u - \Pi_h u)'(x) = 0$. After some computation we get:

$$\begin{aligned} 0 = {} & 2(u - \Pi_h u)(x) + \frac{(a-x)^2}{2} u''\big(x + t_1(a-x)\big) \\ & + \frac{(b-x)^2}{2} u''\big(x + t_2(b-x)\big) \end{aligned}$$

and

$$\big|(u - \Pi_h u)(x)\big| \leqslant \frac{1}{2}\left(\left|\frac{(a-x)^2}{2}\right| + \left|\frac{(b-x)^2}{2}\right|\right) \max_{[a,b]} |u''|.$$

Then

$$\big|(u - \Pi_h u)(x)\big| \leqslant \frac{1}{4} \max_{\xi \in I}\big((a-\xi)^2 + (b-\xi)^2\big) \max_{[a,b]} |u''|.$$

The maximum is reached for $\xi_0 = \frac{(a+b)}{2}$, this implies, $\forall \xi \in I$:

$$\big|e(\xi)\big| = \big|(u - \Pi_h u)(\xi)\big| \leqslant \frac{(b-a)^2}{8} \max_{[a,b]} |u''|. \tag{3}$$

This estimate, after it has been modelled in terms of continuous functions, will contribute to the continuous problem statement.

2.3. Optimal metric

2.3.1. Optimality condition for norm L^α

The interpolation error vanishes on each vertex. Its maximal value inside each element is estimated by (3). An asymptotic extension would also provide something like the right-hand side of (3) as first term. We propose to represent the interpolation error in the continuous setting by a simplified function inspired from these analyses. This process is a modelling process. It is motivated by the need of a more analysable mathematical formulation. We assume that the function u is smooth, that its second derivative u'' is everywhere strictly positive, and that meshes that we consider are enough fine to allow the second-order term of the interpolation error to represent well the whole error. Let us define the continuous local $\mathcal{P}_1$-interpolation error as:

$$\left|e_{\mathcal{M}}(x)\right| = \left(d_{\mathcal{M}}(x)\right)^{-2}\left|u''(x)\right|, \tag{4}$$

where $d_{\mathcal{M}}(x)$ is the node density of the mesh, or equivalently the inverse local mesh size, i.e., the inverse of $m_{\mathcal{M}}(x)$. We want now to find the minimum with respect to metric $\mathcal{M}$ in a set $\mathcal{U}$, of the L^α norm $(0 < \alpha < \infty)$ of the error $e_{\mathcal{M}}$:

$$\min_{\mathcal{M}\in\mathcal{U}} \mathcal{E}_\alpha(\mathcal{M}), \quad \text{with } \mathcal{E}_\alpha(\mathcal{M}) = \left(\left|e_{\mathcal{M}}(x)\right|\right)^\alpha_{L^\alpha} = \int_a^b \left(d_{\mathcal{M}}(x)^{-2}\left|u''(x)\right|\right)^\alpha \mathrm{d}x, \tag{5}$$

with respect to $d_{\mathcal{M}}$, $\mathcal{U}$ is an open subset of L^2 such that any metric in $\mathcal{U}$ is such that $d_{\mathcal{M}} > 0$ and $d_{\mathcal{M}}^{-2\alpha}$ is of bounded integral. For a node density tending to infinity, the error tends to zero. Let us recall that a sequence of 1D metrics $\mathcal{M}_n$ having n nodes gives a *κth order convergence* in L^α norm if the corresponding error satisfies:

$$\left(\left|e_{\mathcal{M}_n}(x)\right|\right)_{L^\alpha} \leqslant \text{const} \cdot n^{-\kappa}. \tag{6}$$

If we can state such a property for the metric model, this would be a good indication that the κth order convergence is satisfied by meshes built from these metrics.

In order to avoid finding the trivial infinitely fine solution, the space of admissible metrics is restricted prescribing the number of nodes:

$$\forall \mathcal{M} \in \mathcal{U}, \quad C(\mathcal{M}) = \overline{C}(d) = \int_a^b d(x)\,\mathrm{d}x = N. \tag{7}$$

This gives a linear constraint for variable d. In order to get (at least formally) optimality condition, we can differentiate the functional of (5) with respect to d:

$$-2\alpha \int_a^b d^{-2\alpha-1}\left(|u''|\right)^\alpha \delta d\,\mathrm{d}x \geqslant 0, \quad \forall \delta d\colon \int_a^b \delta d\,\mathrm{d}x = 0.$$

Thus

$$d_{\text{opt}}(x) = K_1.\left|u''(x)\right|^{\frac{\alpha}{2\alpha+1}}$$

where K_1 is a constant which we can determine by taking into account the constraint (7), we get:

$$d_{\text{opt}}(x) = \frac{N}{\int |u''|^{\frac{\alpha}{2\alpha+1}}\,\mathrm{d}x'}\left|u''(x)\right|^{\frac{\alpha}{2\alpha+1}} \tag{8}$$

or, in terms of the local mesh size:

S0168-9274(05)00062-0/FLA AID:1766 Vol.●●●(●●●) anm1766 [DTD5] P.6 (1-29)
APNUM:m2 v 1.36 Prn:25/03/2005; 8:35 by:ML p. 6

$$m_{\text{opt}}(x) = \frac{\int |u''|^{\frac{\alpha}{2\alpha+1}}\,\mathrm{d}x'}{N}\left|u''(x)\right|^{\frac{-\alpha}{2\alpha+1}}. \tag{9}$$

The minimum of the functional writes:

$$\left(\mathcal{E}_\alpha^{\text{opt}}\right)^\alpha = \frac{1}{N^{2\alpha}}\left(\int_a^b |u''|^{\frac{\alpha}{2\alpha+1}}\,\mathrm{d}x'\right)^{2\alpha}\left(\int_a^b \left|u''(x)\right|^{\frac{1}{2\alpha+1}}\,\mathrm{d}x\right). \tag{10}$$

Remark 1. The smoothness of u is important in this analysis but u can be replaced in practice by a smoother function. Since the Hessian of the functional is always positive, the solution d_{opt} is the unique global optimum.

Remark 2. The local mesh size, naturally inverse proportional to the number of nodes, is defined by (9) only if the second derivative u'' never vanishes. In practice, we replace $|u''|$ by $\max(\varepsilon, |u''|)$, with a small positive ε.

2.3.2. Examples

- For L^1 norm: this is a rather usual norm in image processing, we get

$$m_{\text{opt}}^1(x) = \frac{\int |u''|^{1/3}\,\mathrm{d}x'}{N}\left|u''(x)\right|^{-1/3}. \tag{11}$$

- For L^2 norm, which is the natural option for PDE's, we get

$$m_{\text{opt}}^2(x) = \frac{\int |u''|^{2/5}\,\mathrm{d}x'}{N}\left|u''(x)\right|^{-2/5}. \tag{12}$$

- For the case of L^∞ norm, due to insufficient smoothness, we cannot get an optimality condition by differentiating the functional. Instead, we can get a formal one by making the power coefficient in (9) tend to infinity:

$$m_{\text{opt}}^\infty(x) = \frac{\int |u''|^{1/2}\,\mathrm{d}x'}{N}\left|u''(x)\right|^{-1/2}. \tag{13}$$

Remark 3. In the last case, introducing d_{opt}^∞:

$$d_{\text{opt}}^\infty(x) = \frac{N}{\int |u''|^{1/2}\,\mathrm{d}x'}\left|u''(x)\right|^{1/2} \tag{14}$$

in (4) gives a uniform local error,

$$\left|e_{\mathcal{M}}^\infty(x)\right| = \frac{(\int |u''|^{1/2}\,\mathrm{d}x')^2}{N^2} \quad \forall x. \tag{15}$$

It is not a scoop that the L^∞ norm of error is formally minimum when the local error is uniform. This is an option referred in the literature as the error equidistribution, used in [7,13]. We rediscuss that option in Remark 5 in the sequel.

2.4. Convergence order of the continuous metric model

If we take the αth root of expression (10), we get:

$$\mathcal{E}_\alpha^{\text{opt}} = \frac{1}{N^2}\left(\int_a^b |u''|^{\frac{\alpha}{2\alpha+1}}\,\mathrm{d}x'\right)^2 \left(\int_a^b \left|u''(x)\right|^{\frac{1}{2\alpha+1}}\,\mathrm{d}x\right)^{1/\alpha}. \tag{16}$$

Since the two integrals are bounded, this shows that the optimal error decreases as the inverse of square of the number of nodes. According to (6), this expresses the second-order convergence (for $\mathcal{P}_1$ interpolation) of the metric sequence obtained by the present adaption strategy. This is not surprising since the function u is assumed to have continuous second derivatives, and the same property also holds for a sequence of uniform meshes.

Let us examine how to look for an optimal metric in the case of a function u having a *discontinuity*. More precisely, u is bounded and smooth on two parts $[a, c]$ and $[c, b]$ of the interval, but is discontinuous at point c with a nonzero step.

We choose to represent the $\mathcal{P}_1$ interpolation error as:

$$\int_a^b \left|e_{\mathcal{M}}(x)\right|^\alpha \mathrm{d}x' = \int_a^b \left(m^2\left|u''_\delta(x)\right|\right)^\alpha \mathrm{d}x$$

$$\text{with } u''_\delta(x) = \delta^{-2}\bigl(u(x+\delta) - 2u(x) + u(x-\delta)\bigr), \tag{17}$$

where δ is assumed to be smaller than m. Using this error model is justified by the following remarks:

- on the element $[x_i, x_{i+1}]$ containing the discontinuity, the interpolation error $\int_{x_i}^{x_{i+1}} |\Pi_h u - u|^\alpha\,\mathrm{d}x$ is smaller than $\int_{x_i}^{x_{i+1}} \operatorname{meas}([x_i, x_{i+1}])^2 |u''_\delta|^\alpha\,\mathrm{d}x$,
- u''_δ is close to $\frac{\partial^2 u}{\partial x^2}$ where u is regular.

Moreover, we observe that u''_δ is of the order of δ^{-2} for x in $[c-\delta, c+\delta]$. Then for γ such that $0 < \gamma \leqslant 1/2$:

$$\|u''_\delta\|_{L^\gamma} \quad \text{is bounded independently of } \delta, \tag{18}$$

and for $\gamma > 1/2$:

$$\|u''_\delta\|_{L^\gamma} \quad \text{is unbounded for } \delta \to 0. \tag{19}$$

According to Remark 1, we can replace the term $|u''_\delta|$ by a smooth approximation of it, that satisfies the above properties. Let us restrict our calculus of variations to the L^2 case ($\alpha = 2$). The resulting optimal error writes:

$$\mathcal{E}_2^{\text{opt}} = \frac{1}{N^2}\left(\int_a^b |u''_\delta|^{2/5}\,\mathrm{d}x'\right)^2 \left(\int_a^b \left|u''_\delta(x)\right|^{1/5}\mathrm{d}x\right)^{1/2} \leqslant \frac{K_2}{N^2}$$

S0168-9274(05)00062-0/FLA AID:1766 Vol.●●●(●●●)
APNUM:m2 v 1.36 Prn:25/03/2005; 8:35
anm1766
[DTD5] P.8 (1-29)
by:ML p. 8

where K_2 is a bounded constant, due to (18). We deduce that the proposed adaptive strategy is also of second-order accuracy for this discontinuous case.

Remark 4. The same analysis can be done with a more accurate interpolation, that is typically with an error model of κth order:

$$\left|e_{\mathcal{M}}(x)\right| = \left(d_{\mathcal{M}}(x)\right)^{\kappa}\left|u^{(\kappa)}\right|,$$

where $u^{(\kappa)}$ holds either for the κ-derivative of u or for a differential quotient close to it. In the second case, the differential quotient is bounded in $L^{1/\kappa}$. In that case, in the optimal error appears a maximal power of the differential quotient which is equal to $\frac{\alpha}{\kappa\alpha+1}$. Since this is always smaller than $1/\kappa$, κ-order accuracy on a discontinuous function is again obtained.

On this basis, extensions to $h-p$ adaptation can be designed.

Remark 5. In this discontinuous case, making α tend to infinity in order to try to get information concerning the L^∞ case is definitively deceitful. It tends to say that L^∞ second-order convergence also holds as a limiting case. But the initial assumption that we can represent the L^∞ error with an integral of form (5) is wrong. The L^∞ error between a fixed discontinuous function and continuous approximations simply cannot tend to zero.

3. The 2D case

We propose a 2D extended model for the $\mathcal{P}_1$ interpolation error and then apply again a variation calculus.

3.1. Definitions and notations

Let u be a twice continuously differentiable function from a subset Ω of R^2 in R. The Hessian of u is denoted by

$$\mathcal{H}_u = \begin{pmatrix} \frac{\partial^2 u}{\partial x^2} & \frac{\partial^2 u}{\partial x.\partial y} \\ \frac{\partial^2 u}{\partial x.\partial y} & \frac{\partial^2 u}{\partial y^2} \end{pmatrix}, \tag{20}$$

$\mathcal{H}_u$ is diagonalizable through a rotation $\mathcal{R}_u$ passing from the usual (x, y) coordinate system to a system (ξ, η):

$$\mathcal{H}_u = \mathcal{R}_u \widehat{\mathcal{H}}_u \mathcal{R}_u^{-1} = \mathcal{R}_u \begin{pmatrix} \lambda_1 & 0 \\ 0 & \lambda_2 \end{pmatrix} \mathcal{R}_u^{-1}, \tag{21}$$

where

$$\lambda_1 = \frac{\partial^2 u}{\partial \xi^2}, \qquad \lambda_2 = \frac{\partial^2 u}{\partial \eta^2}, \qquad |\lambda_1| \geqslant |\lambda_2|. \tag{22}$$

The family of metrics $\mathcal{M}$ we shall consider involves a tensor field depending on (x, y) and defined as follows a rotation $\mathcal{S}_{\mathcal{M}}$ and its inverse $\mathcal{S}_{\mathcal{M}}^{-1}$:

S0168-9274(05)00062-0/FLA AID:1766 Vol.●●●(●●●) APNUM:m2 v 1.36 Prn:25/03/2005; 8:35 anm1766 [DTD5] P.9 (1-29) by:ML p. 9

$$\mathcal{M}(x,y)=\mathcal{S}_{\mathcal{M}}^{-1}\begin{pmatrix} \frac{1}{m_{\mathcal{M},\theta}}^2 & 0 \\ 0 & \frac{1}{m_{\mathcal{M},\zeta}}^2 \end{pmatrix}\mathcal{S}_{\mathcal{M}}, \tag{23}$$

where $\mathcal{S}_{\mathcal{M}}$, $m_{\mathcal{M},\theta}$, and $m_{\mathcal{M},\zeta}$ depend on x and y. Similarly to the 1D case, the length $L_{\mathcal{M}}(\vec{cd})$ of a vector $\vec{cd}$ in metric $\mathcal{M}$ is defined as follows:

$$L_{\mathcal{M}}(\vec{v})=\int_0^1 \sqrt{\vec{v}.\mathcal{M}.\vec{v}}\big(x'\vec{c}+(1-x')\vec{d}\big)\,\mathrm{d}x'. \tag{24}$$

Ideally, in a mesh defined by the metric $\mathcal{M}$, any edge $\vec{e}$ is exactly of length $L_{\mathcal{M}}(\vec{e})$ equal to 1. The coefficients $m_{\mathcal{M},\theta}$, and $m_{\mathcal{M},\zeta}$ are the local mesh sizes of $\mathcal{M}$ in each of the two directions $\theta_{\mathcal{M}}$ and $\zeta_{\mathcal{M}}$ defined by the rotation $\mathcal{S}_{\mathcal{M}}$. We omit the index $\mathcal{M}$ for simplifying notations. Quantities $\frac{1}{m_\theta}$ and $\frac{1}{m_\zeta}$ represent the number of mesh elements by unit length following respectively axes θ and ζ. In a similar way to the 1D case, we associate to a metric $\mathcal{M}$ the *local density of nodes* d (again index $\mathcal{M}$ is omitted):

$$d(x,y)=\frac{1}{m_\theta}.\frac{1}{m_\zeta} \tag{25}$$

and the total number of nodes defined as the integral of mesh density,

$$C(\mathcal{M})=\int_\Omega \frac{1}{m_\theta}\frac{1}{m_\zeta}\,\mathrm{d}x\,\mathrm{d}y. \tag{26}$$

The soundness of these definitions is easily checked for structured meshes. In the 2D case, a sequence of 2D metrics $\mathcal{M}_n$ having $C(\mathcal{M}_n)=n$ nodes gives a *κth order convergence* for a given error norm $|e_{\mathcal{M}_n}(x)|_{L^\alpha}$ if we have:

$$\big|e_{\mathcal{M}_n}(x)\big|_{L^\alpha}\leqslant \text{const}\cdot n^{-\kappa/2}. \tag{27}$$

3.2. Rough upper bound

The justification of a 2D interpolation error model needs to come back to estimates a little more deeply than for the 1D case. We present now calculations that are slight modifications of analyses available in the literature. To any triangulation $\mathcal{T}_h$ of Ω corresponds an $\mathcal{P}_1$ interpolation of u that we denote by $\Pi_h u$. For the local error analysis, we consider $K=[a,b,c]$, a triangle of $\mathcal{T}_h$ of diameter $h_{\max}$. Functions u and $\Pi_h u$ coincide in a, b and c. Let us estimate the error $e=u-\Pi_h u$ on $K=[a,b,c]$. Let us write $(u-\Pi_h u)$ in the neighboring of a. Symbol z holds for a point od K:

$$(u-\Pi_h u)(a)=(u-\Pi_h u)(z)+\big\langle\vec{za},\nabla(u-\Pi_h u)(z)\big\rangle+\frac{1}{2}\big\langle\vec{az},H_u(z+t_1\vec{za})\vec{az}\big\rangle,$$

where t_1 is between 0 and 1 and depends on z and a and where we denote by $\langle\vec{v},H(\cdot)\vec{v}\rangle$ the scalar product related to $H(\cdot)$. Similarly, for b and c, we get:

$$(u-\Pi_h u)(b)=(u-\Pi_h u)(z)+\big\langle\vec{zb},\nabla(u-\Pi_h u)(z)\big\rangle+\frac{1}{2}\big\langle\vec{bz},H_u(z+t_2\vec{zb})\vec{bz}\big\rangle,$$

$$(u-\Pi_h u)(c)=(u-\Pi_h u)(z)+\big\langle\vec{zc},\nabla(u-\Pi_h u)(z)\big\rangle+\frac{1}{2}\big\langle\vec{cz},H_u(z+t_3\vec{zc})\vec{cz}\big\rangle.$$

S0168-9274(05)00062-0/FLA AID:1766 Vol.●●●(●●●) anm1766 [DTD5] P.10 (1-29)
APNUM:m2 v 1.36 Prn:25/03/2005; 8:35 by:ML p. 10

In order to have an upper bound of $e = (u - \Pi_h u)$, we look for a point z where the extremum is attained. If z is in K then

$$\nabla(u - \Pi_h u)(z) = 0,$$

or

$$\langle \vec{\text{vec}}, \nabla(u - \Pi_h u)(z)\rangle = 0,$$

for any $\vec{\text{vec}}$ in R^2 or in K. Using the three above extension and remaking that $e(a) = e(b) = e(c) = 0$, we get:

$$0 = (u - \Pi_h u)(z) + \frac{1}{2}\langle \vec{az}, H_u(z + t_1\vec{za})\vec{az}\rangle,$$
$$0 = (u - \Pi_h u)(z) + \frac{1}{2}\langle \vec{bz}, H_u(z + t_2\vec{zb})\vec{bz}\rangle,$$
$$0 = (u - \Pi_h u)(z) + \frac{1}{2}\langle \vec{cz}, H_u(z + t_3\vec{zc})\vec{cz}\rangle$$

and by addition

$$0 = 3(u - \Pi_h u)(z) + \frac{1}{2}\langle \vec{az}, H_u(z + t_1\vec{za})\vec{az}\rangle + \frac{1}{2}\langle \vec{bz}, H_u(z + t_2\vec{zb})\vec{bz}\rangle + \frac{1}{2}\langle \vec{cz}, H_u(z + t_3\vec{zc})\vec{cz}\rangle.$$

Let M be a real number such that

$$M = \max_{z\in K}\left(\max_{\vec{\text{vec}}\in R^2} \frac{|\vec{\text{vec}}, H_u(z)\vec{\text{vec}}|}{\|\vec{\text{vec}}\|^2}\right).$$

Then

$$\left|(u - \Pi_h u)(z)\right| \leqslant \frac{1}{6}\left(\|\vec{az}\|^2 + \|\vec{bz}\|^2 + \|\vec{cz}\|^2\right)M.$$

By definition,

$$z = \lambda_a a + \lambda_b b + \lambda_c c,$$

with

$$\lambda_a + \lambda_b + \lambda_c = 1.$$

Thus

$$\vec{az} = \lambda_b\vec{ab} + \lambda_c\vec{ac}, \qquad \vec{bz} = \lambda_c\vec{bc} + \lambda_a\vec{ba}, \qquad \vec{cz} = \lambda_a\vec{ca} + \lambda_b\vec{cb}.$$

We deduce that

$$\begin{aligned}
&\|\vec{az}\|^2 + \|\vec{bz}\|^2 + \|\vec{cz}\|^2 \\
&\quad\leqslant \left(\lambda_a^2 + \lambda_b^2\right)\|\vec{ab}\|^2 + \left(\lambda_a^2 + \lambda_c^2\right)\|\vec{ac}\|^2 + \left(\lambda_b^2 + \lambda_c^2\right)\|\vec{bc}\|^2 \\
&\qquad + 2(\lambda_a\lambda_b)\left|\langle\vec{ca}, \vec{cb}\rangle\right| + 2(\lambda_a\lambda_c)\left|\langle\vec{ba}, \vec{bc}\rangle\right| + 2(\lambda_b\lambda_c)\left|\langle\vec{ab}, \vec{ac}\rangle\right|.
\end{aligned}$$

If we denote by L the length of the largest edge, then:

$$\|\vec{az}\|^2 + \|\vec{bz}\|^2 + \|\vec{cz}\|^2 \leqslant 2\left(\lambda_a^2 + \lambda_b^2 + \lambda_c^2 + \lambda_a\lambda_b + \lambda_a\lambda_c + \lambda_b\lambda_c\right)L^2.$$

S0168-9274(05)00062-0/FLA AID:1766 Vol.●●●(●●●) anm1766 [DTD5] P.11 (1-29)
APNUM:m2 v 1.36 Prn:25/03/2005; 8:35 by:ML p. 11

One easily verifies that the extremum is reached at:

$$\lambda_a = \lambda_b = \lambda_c = \frac{1}{3}$$

and thus the upper bound writes:

$$\left|(u - \Pi_h u)(z)\right| \leqslant \frac{2}{9} L^2 M. \tag{28}$$

This result suggests the form of the upper bound to get in the case of an arbitrary dimension d:

$$\left|(u - \Pi_h u)(z)\right| \leqslant \frac{1}{2}\frac{1}{1+d}\left(\frac{d(d+1)}{(d+1)^2} + 2\frac{d(d-1)}{2}\frac{d+1}{d+1}^2\right) L^2 M \leqslant \frac{1}{2}\left(\frac{d}{1+d}\right)^2 L^2 M.$$

We return to the case where the extremum is not reached in K. Then it corresponds to an edge, let us say the edge ab. The gradient vanishes on ab and it follows that:

$$0 = 2(u - \Pi_h u)(z) + \frac{1}{2}\langle \vec{az}, H_u(z + t_1\vec{za})\vec{az}\rangle + \frac{1}{2}\langle \vec{bz}, H_u(z + t_2\vec{zb})\vec{bz}\rangle.$$

Let M such that

$$M = \max_{z \in \vec{ab}}\left(\max_{\vec{\text{vec}} \in ab} \frac{|\langle \vec{\text{vec}}, H_u(z)\vec{\text{vec}}\rangle|}{\|\vec{\text{vec}}\|^2}\right), \tag{29}$$

then

$$\left|(u - \Pi_h u)(z)\right| \leqslant \frac{1}{4}\left(\|\vec{az}\|^2 + \|\vec{bz}\|^2\right) M.$$

Since $z = \lambda_a a + \lambda_b b$, we recover the upper bound established in one dimension:

$$\left|(u - \Pi_h u)(z)\right| \leqslant \frac{1}{8}\left(\|\vec{ab}\|^2\right) M.$$

And then:

$$\left|(u - \Pi_h u)(z)\right| \leqslant \frac{1}{8} L^2 M, \quad M \text{ defined by (29).} \tag{30}$$

This result is better than (28) but does not provide any information concerning the possible anisotropy of the function. It cannot be used in order to prescribe mesh stretching.

3.3. *An anisotropic upper bound*

Anisotropic upper bounds are the topic of many current studies, see, for example, [20]. We give here a result adapted to our needs. The notations of previous section are kept. Let us assume that the point z where the maximum is attained is closer to a than to b or c. We assume also that z is in K (not on an edge). We denote by a' the intersection point between az and the edge facing a in K, i.e., bc (Fig. 1). We develop e from a:

$$e(a) = (u - \Pi_h u)(a) = (u - \Pi_h u)(z) + \left\langle \vec{za}, \nabla(u - \Pi_h u)(z)\right\rangle + \int_0^1 (1-t)\left\langle \vec{za}, H_u(z + t\vec{za})\vec{az}\right\rangle \mathrm{d}t.$$

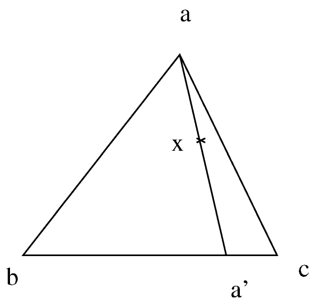

Fig. 1. Anisotropic error analysis.

Since z is closer to a, the number λ, such that $\vec{az} = \lambda\vec{aa'}$, is smaller than $\frac{2}{3}$:

$$\left|e(z)\right| = \left|\int_0^1 (1-t)\lambda^2 \langle \vec{aa'}, H_u(a+t\vec{za})\vec{aa'}\rangle \,\mathrm{d}t\right|,$$

$$\left|e(z)\right| \leqslant \frac{4}{9}\left|\int_0^1 (1-t)\langle \vec{aa'}, H_u(a+t\vec{za})\vec{aa'}\rangle \,\mathrm{d}t\right|,$$

$$\left|e(z)\right| \leqslant \frac{4}{9}\left|\int_0^1 (1-t)\,\mathrm{d}t\right| \max_{t\in[0,1]}\left|\langle \vec{aa'}, H_u(a+t\vec{za})\vec{aa'}\rangle\right|.$$

Then

$$\left|e(z)\right| \leqslant \frac{2}{9}\max_{z'\in\vec{aa'}}\left|\langle \vec{aa'}, H_u(z')\vec{aa'}\rangle\right|. \tag{31}$$

The case where z is located on an edge, let us say edge ab, will eventually lead to the same upper bound:

$$\left|e(z)\right| \leqslant \frac{1}{8}\max_{z'\in ab}\left|\langle \vec{ab}, H_u(z')\vec{ab}\rangle\right|. \tag{32}$$

The two cases (31) and (32) allow to write the final estimate:

$$\left|e(z)\right| \leqslant \frac{2}{9}\max_{z'\in K}\left|\langle \vec{aa'}, H_u(z')\vec{aa'}\rangle\right|. \tag{33}$$

3.4. Error modelling

For the sake of simplicity we assume that the Hessian eigenvalues λ_1 and λ_2 in (22) have positive and different absolute values. Extension to other cases are evident or will be discussed in the sequel. Let us first study the case of isotropic, i.e., non-stretched, meshes. We consider finding an optimal isotropic metric, i.e., with $m_\theta = m_\zeta = m$ in (23):

$$\mathcal{M}(x,y) = \mathcal{S}_{\mathcal{M}}^{-1}\begin{pmatrix} \frac{1}{m_\theta^2} & 0 \\ 0 & \frac{1}{m_\zeta^2} \end{pmatrix}\mathcal{S}_{\mathcal{M}} = \frac{1}{m^2}\mathrm{Id}. \tag{34}$$

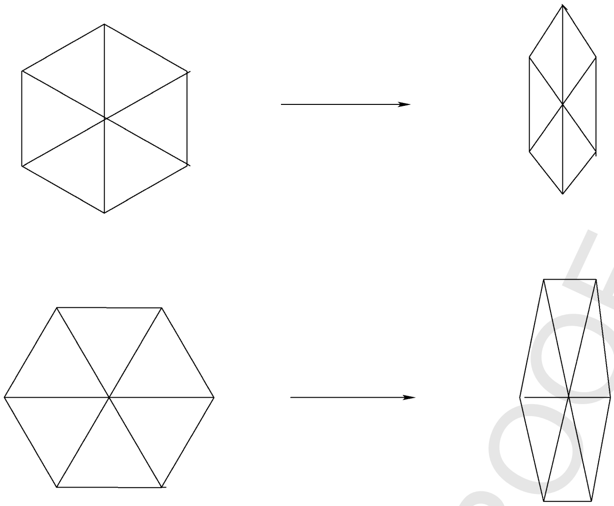

Fig. 2. Stretching of a regular mesh.

It is natural to identify the local mesh size with the largest edge length in estimate (30). We deduce the following error model:

$$e_{\mathcal{M}}(x, y) = m^2(x, y)s(x, y), \qquad s(x, y) = \max\bigl(|\lambda_1|, |\lambda_2|\bigr) \tag{35}$$

where $s(x, y)$ is taken equal to the largest absolute value of eigenmodes (22) of the Hessian of u at point (x, y).

If we investigate anisotropic meshes, the modelling is somewhat more delicate. When considering, for example, the deformation of an equilateral mesh, a mesh quality question arises. Indeed, the same stretching can produce in one case an acute mesh and, in the other one, a mesh involving angles close to π. See Fig. 2.

These two meshes have identical local densities, but the corresponding error is different. This kind of situation is analysed in the literature studying mesh quality. See, for example, [20]. From these works its turns out that the degradation in $\mathcal{L}^\alpha$ interpolation error between the two extremal situations of Fig. 2 can introduce a factor 2 in the error. But in our continuous model, there is no way to distinguish between the two stretchings. We cannot do anything but neglect this kind of event, or, equivalently, assume that obtuse triangles are not considered.

Our metric $\mathcal{M}$ specifies as m_θ the (smallest) segment length length$(\vec{ab})$ (among the segments inside the triangle) in the stretched direction, and as m_ζ the (largest) segment length in the direction orthogonal to the stretched direction. Let us assume that the function u has a uniform Hessian H_u, i.e., a Hessian not depending on space variables x and y. This restricts our investigation to uniform metrics. The mesh is the image of a uniform (equilateral) mesh by an affinity of stretching in the direction specified by the rotation $\mathcal{S}$. Any triangle of the stretched mesh lies inside the ellipse, image of the circumcenter circle for the initial equilateral mesh (Fig. 3).

An upper bound for the length of a segment inside the triangle in a particular direction is the chord of same direction passing by the center of the ellipse. This upper bound can be attained in practice by a particular element verifying approximatively the metric specification. Taking this ellipse E as a model for the local triangle K in the error estimate (33), we observe that the error estimate writes:

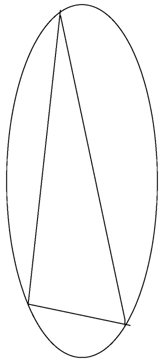

Fig. 3. The ellipse modelling a stretched triangle.

$$e_{\mathcal{M}} = \max_{a,a' \in E} \left| \langle \vec{aa'}, H_u \vec{aa'} \rangle \right|. \tag{36}$$

Let us identify the best rotation (S) for our metric. The right-hand side of (36) will be minimum when the larger axis of the ellipse is aligned with the largest eigenvalue direction of the Hessian, i.e.:

$$\mathcal{S}_{\mathcal{M}} = \mathcal{R}_u. \tag{37}$$

This option is adopted for the general case of non-uniform Hessians in the rest of the paper. The pointwise error estimates can be then written in a simplified form:

$$e_{\mathcal{M}}(x, y) = \left| \frac{\partial^2 u}{\partial \xi^2} \right| . m_\xi^2 + \left| \frac{\partial^2 u}{\partial \eta^2} \right| . m_\eta^2. \tag{38}$$

Remark 6. In practice, the difference between stretching with and without obtuse angles makes sense only at the step when the metric is interpreted into a mesh. Given a metric, shall we build a stretched mesh without or with obtuse angles? The answer depends strongly on the algorithm applied for mesh generation. For example, a mesh adaptation by deformation can produce obtuse angles. But this can be compensated in 2D by diagonal swapping.

3.5. Minimization of the interpolation error (I)

According to (35), the local mesh size is defined as a unique scalar field, $m(x, y)$ or equivalently the node density by area unit $d(x, y) = 1/m^2(x, y)$. The total number of nodes is given by:

$$C(\mathcal{M}) = \int_{\Omega} d(x, y)\, \mathrm{d}x\, \mathrm{d}y. \tag{39}$$

For error modelling, we get inspiration from the above rough estimate:

$$e_{\mathcal{M}}(x, y) = m^2(x, y) s(x, y) = d^{-1}(x, y) s(x, y), \tag{40}$$

where $s(x, y)$ is given in (35). Let us minimize the $\mathcal{L}^\alpha$ norm of this error under the constraint of a number of nodes equal to N:

$$\min_{\mathcal{M}} \int_{\Omega} s^{\alpha} d^{-\alpha}\, \mathrm{d}x\, \mathrm{d}y \tag{41}$$

under the constraint $C(\mathcal{M}) = N$.

The optimality conditions are:

$$-\alpha \int_{\Omega} s^{\alpha} d^{-\alpha-1} \delta d\, \mathrm{d}x\, \mathrm{d}y \leqslant 0 \tag{42}$$

for any δd such that $\int_{\Omega} \delta d\, \mathrm{d}x\, \mathrm{d}y = 0$, or taking into account the constraint:

$$d_{\text{opt}}(x, y) = \frac{N}{\int_{\Omega} s^{\frac{\alpha}{\alpha+1}}\, \mathrm{d}x\, \mathrm{d}y} s(x, y)^{\frac{\alpha}{\alpha+1}}, \tag{43}$$

$$m_{\text{opt}}(x, y) = \frac{(\int_{\Omega} s^{\frac{\alpha}{\alpha+1}}\, \mathrm{d}s)^{1/2}}{N^{1/2}} s(x, y)^{\frac{-\alpha}{2(\alpha+1)}}. \tag{44}$$

Remark 7. Again the case $\alpha = +\infty$ gives $d = s$, that is the error equidistribution option referred in Remark 3.

The corresponding optimal error writes:

$$\mathcal{E}_{\alpha}^{\text{opt}} = \frac{1}{N} \int_{\Omega} s^{\frac{\alpha}{\alpha+1}}\, \mathrm{d}x\, \mathrm{d}y \left(\int_{\Omega} s^{\frac{\alpha}{\alpha+1}}\, \mathrm{d}x\, \mathrm{d}y \right)^{1/\alpha}. \tag{45}$$

For analysing the accuracy order on a discontinuity, we restrict to a function u equal to the following Heavyside function:

$$u(x, y) = 1 \quad \text{if } x > 1, \quad 0 \quad \text{else}. \tag{46}$$

In the same way as in Section 2.4, the local error coefficient s in terms of derivatives is replaced by a local error s_{δ} in terms of differential quotients, which reduces in our particular case to:

$$s_{\delta}(x, y) = \delta^{-2} \left| u(x + \delta, y) - 2u(x, y) + u(x - \delta, y) \right| \tag{47}$$

which is bounded in $L^{1/2}$, but not in L^{γ}, for $\gamma > 1/2$. Now, for $\alpha = 2$, the power of s_{δ} in the integral of the optimal error is $2/3$, then the integral (45) is not bounded and we do not get second-order accuracy.

3.6. Minimization of the interpolation error (II)

Considering an anisotropic family of metrics, we return to the general notations of Sections 3.1–3.3.

3.6.1. Optimization problem

According to Section 3.4, we consider metrics $\mathcal{M}$ that are written:

$$\mathcal{M}(x, y) = \mathcal{R}_u^{-1} \begin{pmatrix} (m_{\xi})^{-2} & 0 \\ 0 & (m_{\eta})^{-2} \end{pmatrix} \mathcal{R}_u \tag{48}$$

and the functional to minimize is the following one:

S0168-9274(05)00062-0/FLA AID:1766 Vol.●●●(●●●) anm1766 [DTD5] P.16 (1-29)
APNUM:m2 v 1.36 Prn:25/03/2005; 8:35 by:ML p. 16

$$\mathcal{E}_\alpha = \int \left(\left| \frac{\partial^2 u}{\partial \xi^2} \right| .m_\xi^2 + \left| \frac{\partial^2 u}{\partial \eta^2} \right| .m_\eta^2 \right)^\alpha \mathrm{d}x\,\mathrm{d}y. \tag{49}$$

The optimal metric minimizes the functional $\mathcal{E}_\alpha$ under the constraint $C(\mathcal{M}) = N$:

$$\min_{\mathcal{M}} \int \left(\left| \frac{\partial^2 u}{\partial \xi^2} \right| .m_\xi^2 + \left| \frac{\partial^2 u}{\partial \eta^2} \right| .m_\eta^2 \right)^\alpha \mathrm{d}x\,\mathrm{d}y \tag{50}$$

under the constraint $\int m_\xi{}^{-1} m_\eta{}^{-1}\,\mathrm{d}x\,\mathrm{d}y = N$.

The optimality system writes:

$$\begin{aligned} &\mathcal{E}'_\alpha(\mathcal{M})\delta\mathcal{M} = 0, \\ &\forall \delta\mathcal{M}, \quad C'(\mathcal{M}_{\mathrm{opt}}).\delta\mathcal{M} = 0. \end{aligned} \tag{51}$$

The second equation can be used for writing a relation between $\mathcal{M}$ and $\mathcal{C}$:

$$\begin{gathered} C'(\mathcal{M}_{\mathrm{opt}}).\delta\mathcal{M} = 0, \\ \Updownarrow \\ \int \frac{-1}{m_\xi}.\frac{\delta m_\eta}{m_\eta^2} + \frac{-1}{m_\eta}.\frac{\delta m_\xi}{m_\xi^2} = 0, \\ \Updownarrow \\ \int \frac{1}{m_\xi}.\delta m_\eta + \frac{1}{m_\eta}.\delta m_\xi = 0. \end{gathered} \tag{52}$$

One can write

$$\begin{pmatrix} \delta m_\xi \\ \delta m_\eta \end{pmatrix} = \psi \begin{pmatrix} -m_\xi \\ m_\eta \end{pmatrix}. \tag{53}$$

Eq. (51) will be verified for any couple $(\delta m_\xi, \delta m_\eta)$ such that (53) holds at least for one scalar function ψ of (x, y).

Let us develop Eq. (51):

$$\int \left(\left| \frac{\partial^2 u}{\partial \xi^2} \right| m_\xi^2 + \left| \frac{\partial^2 u}{\partial \eta^2} \right| .m_\eta^2 \right)^{\alpha-1} \left(\left| \frac{\partial^2 u}{\partial \xi^2} \right| m_\xi \delta m_\xi + \left| \frac{\partial^2 u}{\partial \eta^2} \right| m_\eta \delta m_\eta \right) \mathrm{d}x\,\mathrm{d}y = 0.$$

Due to statement (53) we can replace δm_ξ and δm_η:

$$\int \left(\left| \left| \frac{\partial^2 u}{\partial \xi^2} \right| m_\xi^2 + \left| \frac{\partial^2 u}{\partial \eta^2} \right| .m_\eta^2 \right|^{\alpha-1} \right) \zeta \left(- \left| \frac{\partial^2 u}{\partial \xi^2} \right| m_\xi m_\xi + \left| \frac{\partial^2 u}{\partial \eta^2} \right| m_\eta m_\eta \right) \mathrm{d}x\,\mathrm{d}y = 0.$$

Since m_η, m_ξ and the second derivatives of u do not vanish, this will be zero for any function ψ if:

$$\left| \frac{\partial^2 u}{\partial \xi^2} \right| .m_\xi^2 = \left| \frac{\partial^2 u}{\partial \eta^2} \right| .m_\eta^2. \tag{54}$$

From which we can derive the ratio between m_ξ and m_η

$$\frac{m_\xi}{m_\eta} = \sqrt{\frac{|(\frac{\partial^2 u}{\partial \eta^2})|}{|(\frac{\partial^2 u}{\partial \xi^2})|}}. \tag{55}$$

ARTICLE IN PRESS
S0168-9274(05)00062-0/FLA AID:1766 Vol.●●●(●●●) anm1766 [DTD5] P.17 (1-29)
APNUM:m2 v 1.36 Prn:25/03/2005; 8:35 by:ML p. 17

For the sequel, it will be simpler to express metric $\mathcal{M}$ in terms of the node density d, number of nodes by area unit, and of the local aspect ratio μ:

$$\mathcal{M} = \frac{1}{d}\mathcal{R}_u^{-1}\begin{pmatrix} \mu & 0 \\ 0 & \frac{1}{\mu} \end{pmatrix}\mathcal{R}_u. \tag{56}$$

More precisely we set: $m_\xi = \sqrt{\frac{\mu}{d}}$ and $m_\eta = \sqrt{\frac{1}{\mu d}}$. Constraint (53) becomes:

$$\int \delta d = 0. \tag{57}$$

Condition (51) can now be written:

$$\int \left(\left|\frac{\partial^2 u}{\partial \xi^2}\right| \frac{\mu}{d} + \left|\frac{\partial^2 u}{\partial \eta^2}\right| \frac{1}{\mu d} \right)^{\alpha-1} \left(\left|\frac{\partial^2 u}{\partial \xi^2}\right| \left(\frac{\delta\mu}{d} - \frac{\mu \delta d}{d^2} \right) - \left|\frac{\partial^2 u}{\partial \eta^2}\right| \frac{d\delta\mu + \mu\delta d}{\mu^2 d^2} \right) = 0,$$
$$\forall \delta d \quad \text{such that} \quad \int \delta d = 0 \text{ and } \forall \delta\mu.$$

Let us develop in function of $\delta\mu$ and δd. For $\delta\mu$

$$\int (*)^{\alpha-1} . \left(\left|\frac{\partial^2 u}{\partial \xi^2}\right| \frac{1}{d} - \left|\frac{\partial^2 u}{\partial \eta^2}\right| \frac{1}{\mu^2 d} \right) \delta\mu = 0 \quad \forall \delta\mu,$$

where $(*)$ stands for $|\frac{\partial^2 u}{\partial \xi^2}|\frac{\mu}{d} + |\frac{\partial^2 u}{\partial \eta^2}|\frac{1}{\mu d}$ which, by assumption, never vanishes. We deduce:

$$\left|\frac{\partial^2 u}{\partial \xi^2}\right| \frac{1}{d} - \left|\frac{\partial^2 u}{\partial \eta^2}\right| \frac{1}{\mu^2 d} = 0.$$

From which we get:

$$\mu = \left(\frac{|\frac{\partial^2 u}{\partial \eta^2}|}{|\frac{\partial^2 u}{\partial \xi^2}|} \right)^{1/2}$$

which is (55). For δd:

$$\int (*)^{\alpha-1} \left(\left|\frac{\partial^2 u}{\partial \xi^2}\right| \frac{-\mu}{d^2} + \left|\frac{\partial^2 u}{\partial \eta^2}\right| \frac{-1}{\mu d^2} \right) \delta d = 0.$$

We get then:

$$(*)^{\alpha-1} \frac{1}{d^2} \left(\left|\frac{\partial^2 u}{\partial \xi^2}\right| (\mu) + \left|\frac{\partial^2 u}{\partial \eta^2}\right| \frac{1}{\mu} \right) = Cte$$

or, in other words:

$$\frac{1}{d^{\alpha+1}} \left(\left|\frac{\partial^2 u}{\partial \xi^2}\right| (\mu) + \left|\frac{\partial^2 u}{\partial \eta^2}\right| \frac{1}{\mu} \right)^{\alpha} = Cte.$$

Let us replace μ by its value:

$$d^{\alpha+1} = Cte \left(\left|\frac{\partial^2 u}{\partial \xi^2}\right| . \left|\frac{\partial^2 u}{\partial \eta^2}\right| \right)^{\alpha/2}.$$

We thus get:

$$d = C_\alpha \left(\left|\frac{\partial^2 u}{\partial \xi^2}\right| \cdot \left|\frac{\partial^2 u}{\partial \eta^2}\right| \right)^{\frac{\alpha}{2\alpha+2}},$$

where constant C_α is given by:

$$C_\alpha = \left(\int \left(\left|\frac{\partial^2 u}{\partial \xi^2}\right| \cdot \left|\frac{\partial^2 u}{\partial \eta^2}\right| \right)^{\frac{\alpha}{2\alpha+2}} \mathrm{d}x\, \mathrm{d}y \right)^{-1} N.$$

Finally the square local mesh sizes are given by:

$$m_\xi^2 = C_\alpha^{-1} \left|\frac{\partial^2 u}{\partial \xi^2}\right|^{\frac{-2\alpha-1}{2(\alpha+1)}} \left|\frac{\partial^2 u}{\partial \eta^2}\right|^{\frac{1}{2(\alpha+1)}}, \qquad m_\eta^2 = C_\alpha^{-1} \left|\frac{\partial^2 u}{\partial \xi^2}\right|^{\frac{1}{2(\alpha+1)}} \left|\frac{\partial^2 u}{\partial \eta^2}\right|^{\frac{-2\alpha-1}{2(\alpha+1)}}$$

which means that metric $\mathcal{M}_{\text{opt}}$ is defined by:

$$\mathcal{M}_{\text{opt}} = C_\alpha^{-1} \left(\left|\frac{\partial^2 u}{\partial \xi^2}\right| \cdot \left|\frac{\partial^2 u}{\partial \eta^2}\right| \right)^{\frac{-\alpha}{2\alpha+2}} \mathcal{R}_u^{-1} \begin{pmatrix} (|\frac{\partial^2 u}{\partial \eta^2}|/|\frac{\partial^2 u}{\partial \xi^2}|)^{1/2} & 0 \\ 0 & (|\frac{\partial^2 u}{\partial \xi^2}|/|\frac{\partial^2 u}{\partial \eta^2}|)^{1/2} \end{pmatrix} \mathcal{R}_u. \tag{58}$$

In the case of the $\mathcal{L}^2$ norm, this becomes:

$$\mathcal{M}_{\text{opt},2} = C_2^{-1} \mathcal{R}_u^{-1} \begin{pmatrix} |\frac{\partial^2 u}{\partial \xi^2}|^{-5/6} |\frac{\partial^2 u}{\partial \eta^2}|^{1/6} & 0 \\ 0 & |\frac{\partial^2 u}{\partial \eta^2}|^{-5/6} |\frac{\partial^2 u}{\partial \xi^2}|^{1/6} \end{pmatrix} \mathcal{R}_u. \tag{59}$$

The case of the $\mathcal{L}^\infty$ norm can be *formally* derived by passing to the limit:

$$\mathcal{M}_{\text{opt},\infty} = C_\infty^{-1} \mathcal{R}_u^{-1} \begin{pmatrix} |\frac{\partial^2 u}{\partial \xi^2}|^{-1} & 0 \\ 0 & |\frac{\partial^2 u}{\partial \eta^2}|^{-1} \end{pmatrix} \mathcal{R}_u. \tag{60}$$

And we again get an equidistribution of the integrand of (49).

3.6.2. Accuracy order in L^2

In the case of L^2 norm, the above expressions simplify as follows:

$$C_\alpha = \left(\int \left(\left|\frac{\partial^2 u}{\partial \xi^2}\right| \cdot \left|\frac{\partial^2 u}{\partial \eta^2}\right| \right)^{1/3} \mathrm{d}x\, \mathrm{d}y \right)^{-1} N \tag{61}$$

and

$$m_\xi^2 = C_\alpha^{-1} \left|\frac{\partial^2 u}{\partial \xi^2}\right|^{-5/6} \left|\frac{\partial^2 u}{\partial \eta^2}\right|^{1/6}, \qquad m_\eta^2 = C_\alpha^{-1} \left|\frac{\partial^2 u}{\partial \xi^2}\right|^{1/6} \left|\frac{\partial^2 u}{\partial \eta^2}\right|^{-5/6}. \tag{62}$$

Let us consider the Heavyside function u of (46). The x-wise second derivative is singular and has to be replaced by a differential quotient

S0168-9274(05)00062-0/FLA AID:1766 Vol.●●●(●●●) anm1766 [DTD5] P.19 (1-29)
APNUM:m2 v 1.36 Prn:25/03/2005; 8:35 by:ML p. 19

$$\left|\frac{\partial^2 u}{\partial x^2}\right| \approx \hat{s}_\delta = \mathrm{Max}(s_\delta, \delta), \tag{63}$$

where s_δ is defined from u as in (47). Again this function is in L^γ for any $\gamma \leqslant 1/2$. The y-wise second derivative is uniformly zero, and has to be corrected by:

$$\left|\frac{\partial^2 u}{\partial y^2}\right| \approx \varepsilon, \tag{64}$$

where ε is a small positive cut-off. Then the above calculations become:

$$C_2 = \left(\int \varepsilon^{1/3}\hat{s}_\delta^{1/3}\,\mathrm{d}x\,\mathrm{d}y\right)^{-1} N \tag{65}$$

and

$$m_x^2 = C_2^{-1}\varepsilon^{1/6}\hat{s}_\delta^{-5/6}, \qquad m_y^2 = C_2^{-1}\varepsilon^{-5/6}\hat{s}_\delta^{1/6}. \tag{66}$$

The local error model for L^2 writes as follows:

$$\mathcal{E}_2 = \left(\int \left(\hat{s}_\delta m_x^2 + \varepsilon m_y^2\right)^2 \mathrm{d}x\,\mathrm{d}y\right)^{1/2}. \tag{67}$$

We can replace:

$$\mathcal{E}_2 = N^{-1}\left(\int \varepsilon^{1/3}\hat{s}_\delta^{1/3}\,\mathrm{d}x\,\mathrm{d}y\right)\left(\int \left(\hat{s}_\delta^{1/6}\left(\varepsilon^{1/6}+\varepsilon^{1/6}\right)\right)^2 \mathrm{d}x\,\mathrm{d}y\right)^{1/2},$$

$$\mathcal{E}_2 = 2N^{-1}\varepsilon^{1/2}\left(\int \hat{s}_\delta^{1/3}\,\mathrm{d}x\,\mathrm{d}y\right)^{3/2}. \tag{68}$$

In contrast to the isotropic adaptation, the integral in the optimal error for anisotropic adaptation is bounded. It is then remarkable that the proposed model suggests that isotropic optimal mesh adaption will not produce a second-order accurate method in L^2 while the anisotropic optimal mesh adaption will produce such an accuracy. These predictions are in accordance with the results in [8,9].

4. A few numerical experiments

Several issues of our theory can be enlightened by a few numerical illustrations.

Firstly, the conclusions of our analysis extend to a discrete context only if that discrete context and our models are close enough to each other. It is crucial to check that this happens not only for extremely fine meshes, but for meshes that can be used in practice.

Secondly, we have shown that the metrics and meshes proposed in the literature for solutions of elliptic problems are related in L^∞ error norm. We have proposed for the L^2 case, a different family of optimal meshes. Then it is interesting to validate our assertion that the second family is somewhat optimal, and to study what qualitative differences appear when we shift from L^∞ to L^2.

In order to do this, we have to pass to a discrete context. We recall that optimization is applied to the continuous context. The discrete system is nothing more than a discretization of the continuous optimality system. The steps for building the discrete system consist of:

S0168-9274(05)00062-0/FLA AID:1766 Vol.●●●(●●●) anm1766 [DTD5] P.20 (1-29)
APNUM:m2 v 1.36 Prn:25/03/2005; 8:35 by:ML p. 20

- building the Hessian, either from analytic differentiation, or, preferably for the sequel, by using a background initial mesh, that is fine enough,
- deriving the optimal metric (continuous or on the background mesh).

From this, we get an approximate solution (a metric on the background mesh) of the continuous problem ("find the optimal metric"). This discrete solution is subject to a discretization error related to the coarseness of the background mesh.

Once the discrete metric is obtained, building the adapted mesh is just post-processing. First we describe the post-processing, then we focus on the verification of how the optimality properties of the continuous solution are approximatively satisfied by the discrete solution.

4.1. *Mesh adaptation tool*

All the presented experiments are performed by using the BAMG software [7]. Given a "background" mesh and an analytic function, BAMG first evaluates on the mesh the Hessian of the function by a discrete differentiation formula before generating the mesh according to the metric.

We have modified BAMG in order that the metric be computed from the Hessian according to the above formula. Once the metric is obtained (on nodes of the background mesh), it is used in a mesh regenerator for rebuilding a new mesh following the metrics. The mesh regenerator relies on a Delaunay reconnection in a space mapped by the metric and on vertex addition, again according to the metric. The number of nodes is adjusted when necessary by trial and errors through the modification of the multiplicative coefficient of the metric. Many experiments with BAMG are described in [14].

4.2. *Optimality assessment*

Since the proposed method defines a kind of optimal mesh on the basis of simplified continuous mesh and error models, it is interesting to show on an example how this optimality can appear in a practical case.

We consider the interpolation on the unit disk of the plane of the following function:

$$f(x,y) = 10x^3 + y^3 + \operatorname{atan}\left(\frac{\epsilon}{\sin(5y) - 2x}\right). \tag{69}$$

Let β be a positive parameter, we consider a series of meshes, indexed by β, that all have about 2100 nodes and are adapted according to the following formula:

$$\mathcal{M}_{\text{opt}} = \left(\left|\frac{\partial^2 u}{\partial \xi^2}\right| . \left|\frac{\partial^2 u}{\partial \eta^2}\right|\right)^{\beta} \mathcal{R}^{-1} \begin{pmatrix} (|\frac{\partial^2 u}{\partial \xi^2}|/|\frac{\partial^2 u}{\partial \eta^2}|)^{1/2} & 0 \\ 0 & (|\frac{\partial^2 u}{\partial \eta^2}|/|\frac{\partial^2 u}{\partial \xi^2}|)^{1/2} \end{pmatrix} \mathcal{R}. \tag{70}$$

This family of metrics involves the usual equidistribution or L^∞ metric, for $\beta = 1$ and the theoretically optimal metric for the L^2 norm, for $\beta = 5/6$ for $\epsilon = 0.0001$. We then compute the L^2 error. Outputs are depicted in Fig. 4. The error norm related to $\beta = 5/6$ is the lowest one, and is about three times smaller than those resulting from $\beta = 0.7$ or from $\beta = 1$.

S0168-9274(05)00062-0/FLA AID:1766 Vol.●●●(●●●)
APNUM:m2 v 1.36 Prn:25/03/2005; 8:35
anm1766
[DTD5] P.21 (1-29)
by:ML p. 21

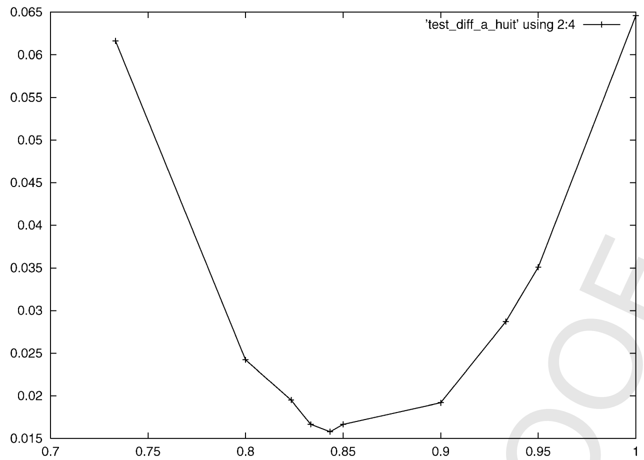

Fig. 4. Optimality of the proposed metric: abscissas are values of the β parameter in the adaptation criterion, ordinates are values of the resulting L^2 interpolation error.

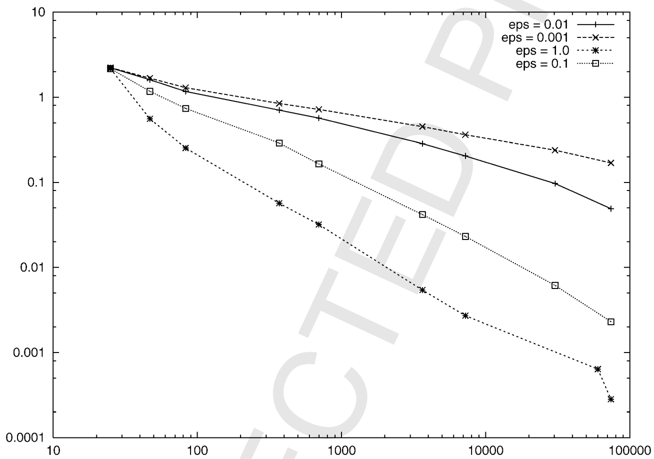

Fig. 5. Convergence of interpolations to exact arctangent functions with uniform mesh refinement, and for different ε. Abscissas are the numbers of nodes in the meshes used, ordinates are values of the resulting L^2 interpolation error.

4.3. *Second-order accuracy*

In [18] it is claimed that for smooth function with *steep gradients*, uniform mesh refinement show numerical second-order convergence only for very fine meshes able to capture all details. It is claimed that, in contrast, best mesh adaptation methods show a property of “early capturing of details”, according to which second-order numerical convergence is observed with meshes with a much smaller number of nodes. The purpose of this section is to show examples for which the early capturing of details occurs.

In order to evaluate this phenomenon, we have considered the interpolation of three functions, f_1, f_2, f_3, f_4, of arctangent type as in (69), with four different “steepness” coefficients: $\epsilon = 1.0, 0.1, 0.01, 0.001$. The mesh convergence is first measured with uniform refinements, Fig. 5. When the function is not steep, second-order convergence is easily obtained. Conversely, we do not observe it for the steepest one, f_4,

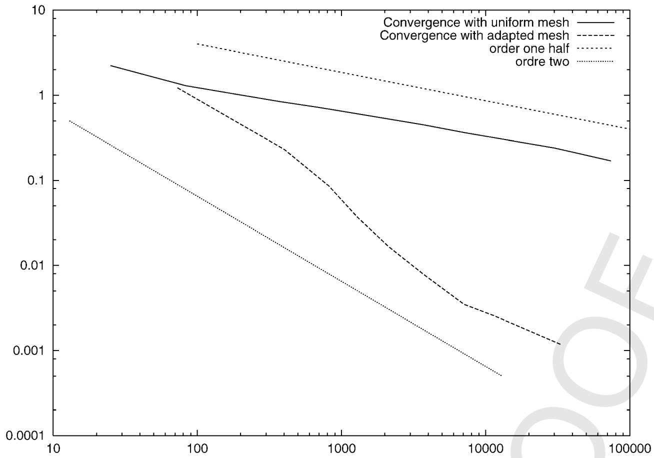

Fig. 6. Convergence to exact arctangent function for $\varepsilon = 0.001$ with optimal adapted meshes, abscissas are numbers of nodes in the meshes used, ordinates are values of the resulting L^2 interpolation error. Comparison with uniform mesh refinement. Upper and lower curves are ideal 0.5th order and 2nd order curves.

even with meshes with almost 100 000 nodes. We now concentrate on the study on f_4 and adapt the meshes by applying the proposed metric. The effect is a much faster convergence, essentially second order, observable for meshes as coarse as of a few hundred nodes (Fig. 6).

4.4. Accuracy order for a discontinuity

In Sections 3.4 and 3.6, we show that for Heavyside functions, the isotropic error model does not have second-order convergence while the anisotropic one has. Now these *a priori* abstract predictions are subject to conditions concerning the representativity of the error model with respect to the practical discretization errors. The purpose of this section is to show one case where theoretical predictions are confirmed by the discrete analog.

We consider the mesh adaptive approximation to a set of two discontinuities, a horizontal one ($y = 0$) and a vertical one ($x = 0$). The optimal metric method is applied. As in the previous section, the BAMG adapted mesh generator is used for building the meshes specified by the different metrics. Sequences of meshes with various numbers of nodes are compared from the standpoint of L^2 interpolation errors for the discontinuities.

First, the isotropic optimal metric is used. An example of mesh is depicted in Fig. 7.

The errors for eleven adapted meshes, with node number ranging from 500 to 200 000 provide a rather clear confirmation of the theoretical prediction given in [8], i.e., that a first-order convergence, not a better one, is obtained by this method (Fig. 8).

Second, the anisotropic optimal metric is used. An example of mesh is depicted in Fig. 9.

The errors for eight adapted meshes, with node number ranging from 150 to 20 000 show a second-order convergence, again as predicted by theory (Fig. 10).

If we gather in Table 1 (a) the best mesh convergence, established with counterexamples in [8], (b) the convergence predicted by the continuous metric model in Sections 3.4 and 3.5, and the results of the experiments of this section, we get perfectly coherent figures.

S0168-9274(05)00062-0/FLA AID:1766 Vol.●●●(●●●)
APNUM:m2 v 1.36 Prn:25/03/2005; 8:35
anm1766
[DTD5] P.23 (1-29)
by:ML p. 23

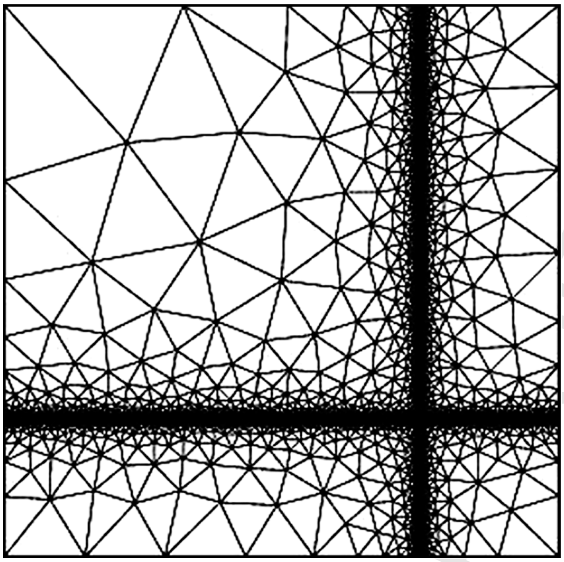

Fig. 7. An example of isotropic adapted mesh for two Heavyside functions.

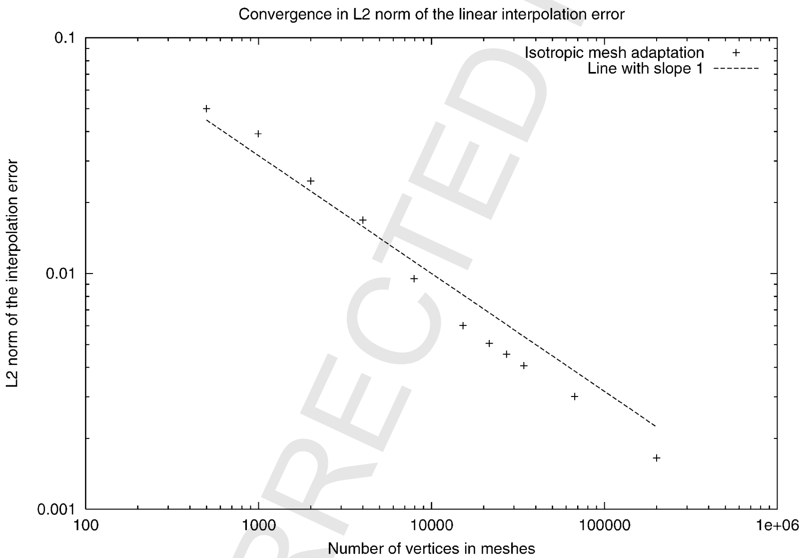

Fig. 8. Convergence in L^2 norm of the P_1 interpolation of two Heavyside functions with an isotropic adaptation strategy.

We end this paragraph by mentioning that second-order convergence is also observed for flow calculations with shocks, see [19].

4.5. Influence of the choice of the norm

As mentioned earlier, the proposed variational analysis takes into account the functional space L^α in which we minimize the interpolation error.

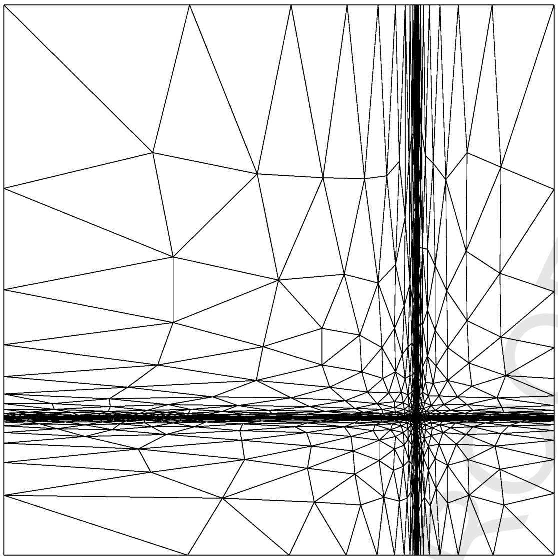

Fig. 9. An example of isotropic adapted mesh for two Heavyside functions.

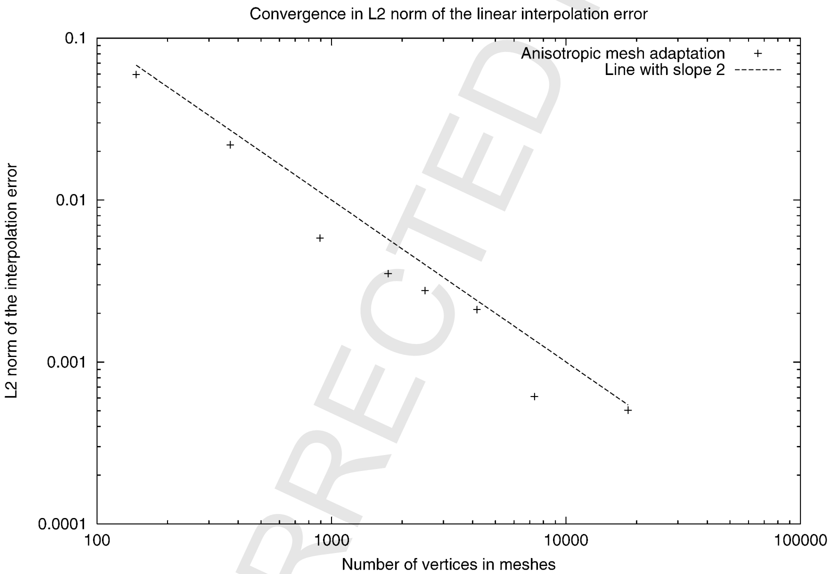

Fig. 10. Convergence in L^2 norm of the P_1 interpolation of two Heavyside functions with an anisotropic adaptation strategy.

The influence of the functional norm will now be studied in relation with the application of a method for image compression.

Indeed, given a function defined on a fine (uniform or not) mesh, a compression could consist of storing it in a smaller mesh, accepting some loss in the accuracy of its definition, as far as the new file is sufficiently small. Mesh adaptive interpolation is an answer to this problem, already used in image processing [16].

Table 1
Convergence in L^2 for a discontinuous function

Convergence order	Isotropic	Anisotropic
Counterexamples [8]	$\leqslant 1$	$\leqslant 2$
Optimal metric theory	<2	2
Optimal metric these experiments	1	2

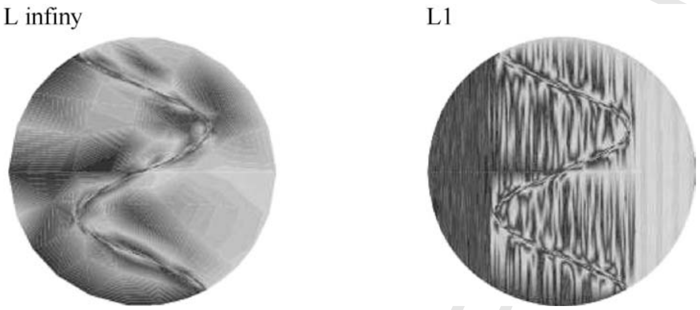

Fig. 11. Representation of a function with the two options, L^∞ (left) and L^2: contours.

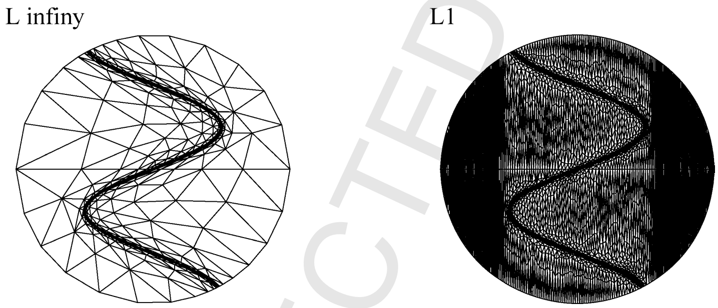

Fig. 12. Representation of a function with the two options, L^∞ (left) and L^2: corresponding meshes.

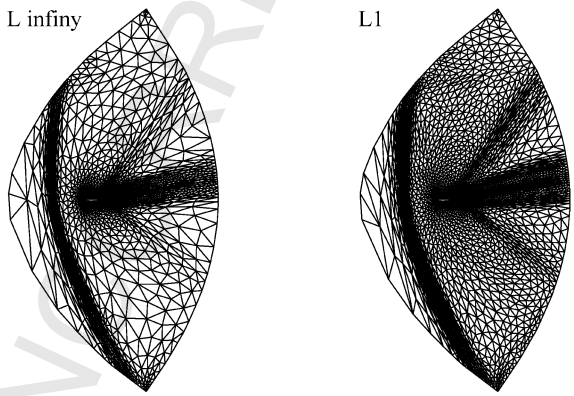

Fig. 13. Mesh-based compression of Mach contours: view of the meshes for L^∞ and L^2 compressions.

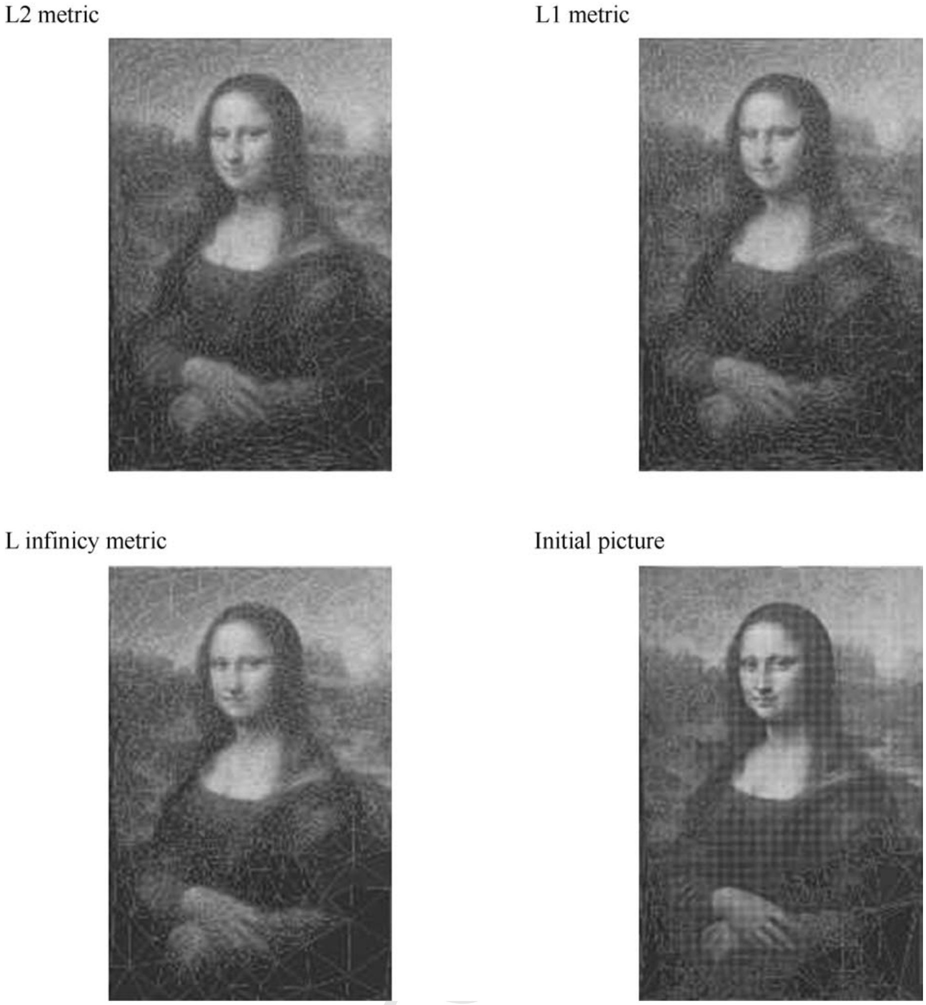

Fig. 14. Mesh-based image compression, global views: initial picture at bottom, L^2 adaptation (top, left), L^1 adaptation (top, right), L^∞ adaptation (bottom, left).

The first example will illustrate the better ability of the L^α option, with small α, to adapt the mesh to the small amplitude details of a function. Let us start with the sum of an arctangent function of amplitude 1, combined this time with a sine function of a ten times lower amplitude

$$f(x, y) = 0.1 * \sin(50x) + \operatorname{atan}\left(\frac{0.001}{\sin(5y) - 2x}\right). \tag{71}$$

We compare two adapted meshes with about 2000 nodes each. The first one is adapted following the error equidistribution principle, in other words, by minimizing the L^∞ error functional. The second one is adapted according to the minimization of the L^2 error norm. We observe that L^2 option restitutes the low amplitude sine oscillation while the L^∞ does not show it at all.

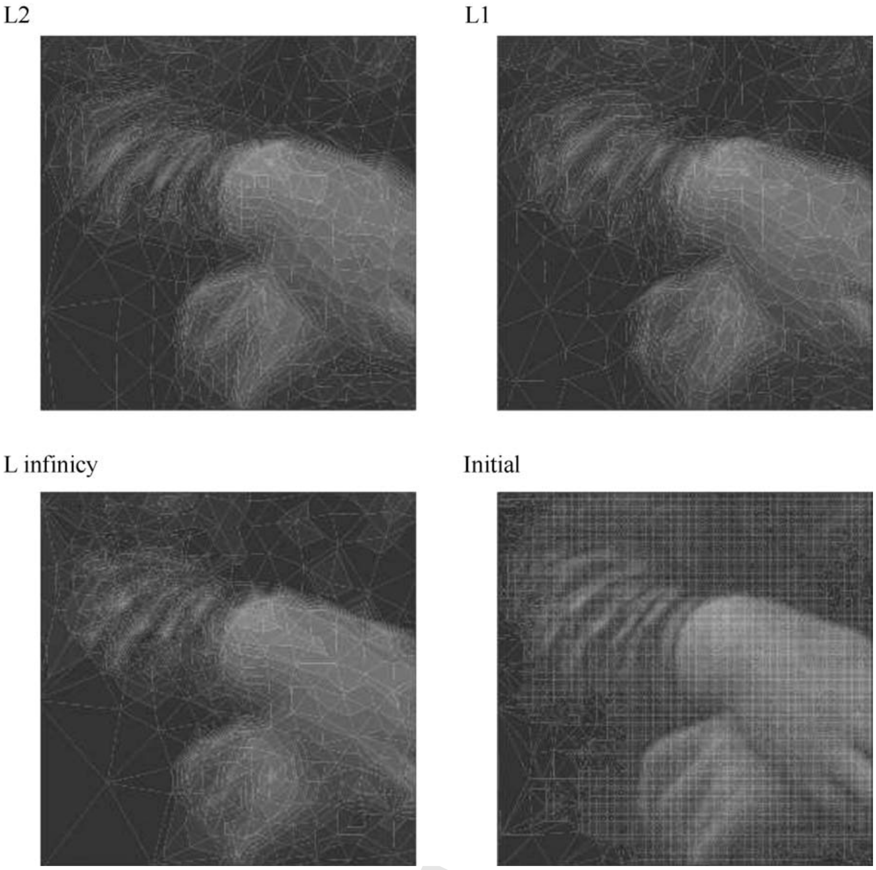

Fig. 15. Mesh-based image compression, zoom: initial picture at (bottom, right), L^2 adaptation (top, left), L^1 adaptation (top, right), L^∞ adaptation (bottom, left).

Mesh-based image compression is particularly useful for storing images produced by numerical finite element computations. As an illustration we consider the compression of the Mach contours of a flow analysis. It is enough to mention it is related to a supersonic flow with different shocks. In Fig. 13 we compare the L^∞ and L^2 adapted meshes. The ramp-like shocks starting from the middle of the airfoil correspond to a much smaller amplitude of variation than the vertical bow shock at left part. We observe that they are nearly ignored by the L^∞ option while it is well followed by the L^1 option.

A last example is the mesh compression of a black and white portrait of Mona Lisa. The initial image we used is depicted as right-bottom of Fig. 14. It was described by a fine adapted mesh of 60 000 vertices resulting from the image processing presented in [11]. The purpose is to compress it to only 5000 vertices with the presented algorithm. We have checked that the compression ratio on postscript files is indeed 12. In that case, the identification of the best approach is not clear. Contrasts are important for the vision and some part of the image (the eyes) are more important than other ones. We note however that some regions with low contrast, such as sleeve and hand, Fig. 15, are better reproduced with the L^2 option.

5. Conclusions

This work explores some capabilities of a continuous setting for mesh adaptation purposes. In this first study, we restrict to the problem of best adaptive mesh for pure interpolation.

A mesh is modelled by a metric. The total number of nodes is a continuous integral of the metric. The continuous interpolation error is modelled with the first term of a Taylor series for the interpolation error. The norm in $L^\alpha, 0 < \alpha < \infty$ of the error model is then minimized. We get a completely explicit expression of the optimal metric in terms of the function to which it is adapted.

When a discontinuous function is considered, the order of accuracy of the adaptation model is predicted. It can help in specifying conditions for practical second-order accuracy.

The usual equirepartition strategy or L^∞ analysis appears as a limiting case which does not enjoy these higher-order convergence properties.

Transposition to the discrete context is demonstrated by a few numerical experiments giving some (yet partial of course) confirmation that the approach is sound, efficient and shows the behaviors predicted by the theory.

This type of analysis has a potential usefulness for several applications:

- *in image compression*: The continuous metric method defines an optimal compression method on an isotropic mesh.
- *in scientific computing*: In a future work we follow the strategy proposed here for extending the present method to the research of an optimal mesh for the solution of a PDE.

Acknowledgements

Thanks to Herve Guillard and Steve Wornom for reading this document, Pascal Frey for providing the data related to Mona Lisa.

References

[1] I. Babuska, W.C. Rheinboldt, A posteriori error estimates for finite element method, Internat. J. Numer. Methods Engrg. 12 (1978) 1597–1615.
[2] I. Babuska, T. Strouboulis, The Finite Element Method and Its Reliability, Clarendo Press, Oxford, 2001.
[3] R. Becker, M. Braack, R. Rannacher, Numerical simulation of laminar flames at low Mach number with adaptative finite elements, Combust. Theory Modelling 3 (1999) 503–534.
[4] H. Borouchaki, P.L. George, Maillage de surfaces paramétriques. Partie I: Aspects théoriques, Technical Report 2928, INRIA Rocquencourt, 1996.
[5] H. Borouchaki, P.L. George, Maillage de surfaces paramétriques. Partie II: Exemples d'applications, Technical Report 2944, INRIA Rocquencourt, 1996.
[6] J. Cabello, R. Lohner, O.-P. Jacquotte, A variational method for the optimization of directionally stretched elements generated by the advancing front method (afm), in: A.S. Arcilla, J. Hauser, P.R. Eiseman, J.F. Thompson (Eds.), Numerical Grid Generation in Computational Field Simulation and Related Fields, Proceedings of the 3rd International Grid Conference, North-Holland, Amsterdam, 1991, p. 521.
[7] M.J. Castro-Diaz, F. Hecht, B. Mohammadi, P.-L. George, Anisotropic adaptative mesh generation in two dimensions for CFD, in: Computationals Fluids Dynamic '96, 1996, pp. 181–192.

[8] Y. Coudiere, B. Palmerio, A. Dervieux, D. Leservoisier, Accuracy barriers in mesh adaptation, Technical Report 4528, INRIA Sophia Antipolis, http://www-sop.inria.fr/rapports/sophia/RR-4528.html, 2002.
[9] A. Dervieux, D. Leservoisier, P.-L. George, Y. Coudière, About theoretical and practical impact of mesh adaptions on approximation of functions and of solution of PDE, Internat. J. Numer. Methods Fluids 43 (2003) 507–516.
[10] M. Fortin (Ed.), Estimations a Posteriori et Adaptation de Maillages, Revue Europeenne des Elements Finis, Special issue, 2000 (partly in French).
[11] P. Frey, Génération de Maillages 3d dans des Ensembles Discrets. Application Biomédicale aux Méthodes d'Éléments Finis, Master's Thesis, University of Strasbourg I, 1993.
[12] P.-J. Frey, P.-L. George, Mesh Generation, Hermes, 2000.
[13] W.G. Habashi, J. Dompierre, Y. Bourgault, D. Ait-Ali-Yahia, M. Fortin, M.-G. Vallet, Anisotropic mesh adaptation: Towards user-independent, mesh-independent and solver-independent CFD solutions: Part I: General principles, Internat. J. Numer. Methods Fluids 32 (2000) 725–744.
[14] D. Leservoisier, Strategies d'Adaptation et de Raffinement de Maillages en Mecanique des Fluides, Ph.D. Thesis, Université Pierre et Marie Curie, 2001.
[15] M. Berzins, A solution based triangular and tetrahedral mesh quality indicator, SIAM J. Sci. Comput. 19 (6) (1998) 2051–2060.
[16] G. Marquant, S. Pateux, C. Labit, Mesh-based scalable image coding with rate-distortion, in: European Signal Processing Conference EUSIPCO 2000, 2000.
[17] B. Palmerio, Coupling mesh and flow in viscous fluid calculations on unstructured triangular finite element, Comput. Fluid Dynamics 6 (1996) 275–290.
[18] B. Palmerio, A. Dervieux, Multimesh and multiresolution analysis for mesh adaptive interpolation, Appl. Numer. Math. 22 (1996) 477–493.
[19] E. Schall, D. Leservoisier, A. Dervieux, B. Koobus, Mesh adaption as a tool for certified computational aerodynamics, Internat. J. Numer. Methods Fluids 45 (2004) 179–196.
[20] J.R. Shewchuk, What is a good linear element? Interpolation, conditioning and quality measures, in: Proceedings of 11th Internat. Meshing Roundtable, Ithaca, NY, 2002, pp. 115–126.
[21] B. Tie, D. Aubry, Adaptative FE strategy for non-linear and coupled structural computation, in: Numerical Methods in Engineering '96, Proceeding of the Second ECCOMAS Conference on Numerical Methods in Engineering, 9–13 September 1996, Wiley, New York, 1999, pp. 516–522.